ORIGINAL ARTICLE

Influence of micro sandblasting on the surface integrity of the AlTiN-coated tools

Zhou Yu[1,2] · Yujuan Dong[3] · Guangming Zheng[1] · Xiuli Jiang[4] · Xiang Cheng[1] · Xianhai Yang[1] · Kaishuo Chang[1] · Xuewei Li[1]

Abstract

Due to the high-efficiency, environmental protection, the low-cost, micro sandblasting technology is used in the surface treatment of the coated tools. The simulation and application of the coated tool micro sandblasting are carried out to reveal the surface treatment mechanism and analyze the influence of sandblasting parameters on the tool surface integrity. The flow field erosion simulation model of abrasive water–air three-phase flow is established. Moreover, the cutting experiments are conducted to verify the effect of micro sandblasting. The results show that the maximum velocity and pressure are obtained at the center of jet flow. The pressure distribution on the target surface has little correlation with the distance to the nozzle. The surface morphology of the AlTiN-coated tool changes obviously after micro sandblasting. Moreover, the low surface roughness R_a of the blasted tool can be obtained at the small sandblasting pressure and time. Additionally, the residual compressive stress on the surface of the AlTiN-coated tool is enhanced after micro sandblasting. The longer cutting time of the AlTiN-coated tool can be obtained at the sandblasting pressure of 0.3 MPa and sandblasting time of 3 s. This work has practical significance for optimizing micro sandblasting process and improving the surface integrity of coated tools.

Keywords Micro sandblasting · Surface integrity · Coated tool · Flow field · Residual stress

1 Introduction

With the development of the modern manufacturing industry, the demand for reworking metal workpiece is increasing. Cutting tools play an important role in it, especially in hard to machine materials. The tool wear is particularly prominent. And the renewal frequency of new tool is increased. So, the cutting cost is increased [1]. To solve such problems, most factories use coated tools. The service life of the coated tool is longer than that of the ordinary tool. And the machined surface quality is improved effectively. But the coated tool with high properties will be more expensive. Due to the significant performance improvement, high-efficiency, low cost, and other advantages, the surface treatment technology is used in the cutting tools. At present, more commonly used surface treatment technologies are mechanical treatment (e.g., sandblasting, grinding, finishing, polishing) and heat treatment (e.g., high energy beam, heat, cryogenic) [2–5]. As one of the surface treatment technologies, the micro sandblasting has been widely used in the surface treatment of coated tools, because of its advantages of simple operation, high-efficiency, safety and pollution-free, and high improvement of cutting performance.

Micro sandblasting is an unconventional subtractive micro-manufacturing technology, which is developed from abrasive jet machining. It is reported that the micro sandblasting process is suitable for treating of some small size workpiece [6], especially for the surface treatment of coated tools. In the wet-type micro sandblasting process, the high-pressure gas is used to push the mixture of abrasive and water to hit the coated tool surface. The size of abrasive is usually measured in microns (5–100 μm). The commonly used abrasive materials mainly include Al_2O_3, AlSi, ZrO_2,

✉ Guangming Zheng
zhengguangming@sdut.edu.cn

1   School of Mechanical Engineering, Shandong University of Technology, 266 West Xincun Road, Zibo 255000, China

2   Goertek Company, 1 Keyuan Wei Road, Qingdao 266300, China

3   College of Preschool Education, Zibo Normal College, 99 Tangjun Ouling Road, Zibo 255130, China

4   Shandong Provincial Institute of Mechanical Design, 129 Jiluo Rode, Jinan 250031, China

SiO$_2$, etc. The sandblasting pressure is 0.1–0.5 MPa, and the sandblasting time is 1–10 s [7]. The impact strengthening effect of abrasive material can strengthen the cohesive strength between coating and substrate.

Micro sandblasting has an important influence on the surface properties, cutting performance, and wear resistance of coated tools. The influences of abrasive particles (Al$_2$O$_3$ and ZnO$_2$) on the hardness and brittleness of coated carbide inserts, tool geometry, and tool life are investigated [8]. They found that micro sandblasting can improve the cutting performance of coated tools. Additionally, micro sandblasting could increase the compressive stress of the coating surface [9]. At the same time, the hardness and brittleness of coating are improved. It is proposed that the micro sandblasting could not only improve the cutting performance, but also improve the tribological performance and adhesion of the coating [10]. During high-speed milling of AISI 4140 (42CrMo4) steel with treated carbide tool, the micro sandblasting can improve the fracture resistance of the carbide tool [11]. While the surface integrity of TiAlN coating is improved after reasonable surface micro sandblasting, the wear resistance of the treated tool is also greatly enhanced when dry turning of Ti6Al4V at high speed [12]. The micro sandblasting is used to treat the CrN-coated samples [13]. It is found that the micro sandblasting process does not have a negative effect on the hardness, adhesion strength, and fatigue resistance of the coated samples. The effect of dry micro sandblasting on the fracture resistance of the PVD-AlTiN-coated carbide cutting tools is also studied [14]. The results show that micro sandblasting can prevent the coating lamination and improve the wear resistance. Other researchers also found that micro sandblasting can improve the life of coated tools [15]. Compared with the commercial tools on the market today, the tool life of the treated tool is three times longer [16]. Compared with the coated tool without any treatment, the hardness of the AlTiN coating is increased after micro sandblasting [7]. According to the appropriate wet micro sandblasting process parameters, CVD-coated tools with good wear resistance can be prepared [16]. The effect of sandblasting on the tribological properties of TiN/MT-TiCN/Al$_2$O$_3$/TiCNO coating is investigated [17]. The micro sandblasting can improve the adhesion of the coating and reduce the appearance of microcracks on the coating surface. It is pointed that the micro sandblasting plays an important role in improving the wear resistance of coating [17]. It is also addressed that micro sandblasting can improve the wear resistance of TiN coating [18]. Additionally, the micro sandblasting can improve the residual compressive stress, reduce the production of microcracks, and increase the fatigue life of the tool [19–21].

The micro sandblasting process is a complex process that the mixture of abrasive and water reaches the tool surface through an air medium [22]. It is difficult to observe the distribution state of the jet in the flow field and analyze the stress change of the treated surface effectively. With the development of computational fluid dynamics, the complex motion of incompressible fluid can be simulated by using technical software [23]. In this work, FLUENT simulation software is used to simulate the process of high-pressure jet impinging on the tool surface. At the same time, the simulation process is verified by micro sandblasting test. The changes in surface morphology and physical properties of the blasted coated tool are studied. The cutting life of the treated tools is also investigated. This research is helpful to set the parameters of tool surface treatment and improve machining efficiency. It can provide some technical reference and guidance for tool post-processing.

2 Material and methods

2.1 Jet structure model

Figure 1a shows the schematic diagram of micro-abrasive water jet. The high-pressure gas pushes the mixture of abrasive and water through the venturi into the nozzle.
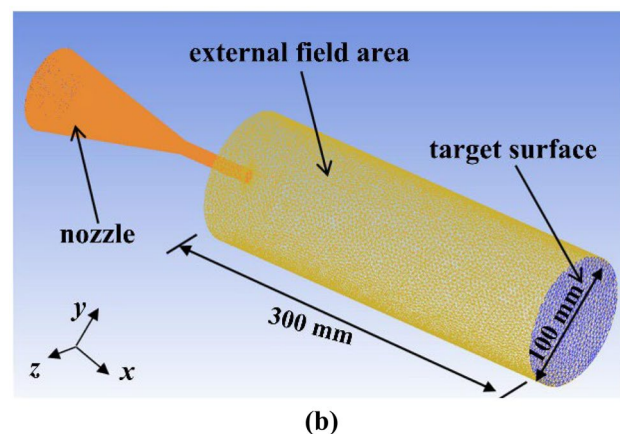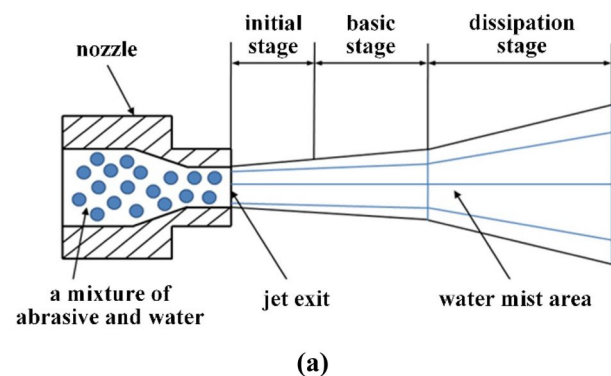

(a)

(b)

Fig. 1 Schematic diagram of **a** micro-abrasive water jet and **b** flow field simulation grid division

And then, the micro-abrasive water jet enters the flow field from the nozzle to reach the target surface. This process is divided into three stages: initial stage, basic stage, and dissipative stage.

In the initial stage, the jet leaves the nozzle and enters the flow field area. The jet formed by abrasive and water have exchange energy with the air medium. The jet flow at the nozzle is in a tight convergence state. At this point, the maximum of the velocity and pressure is obtained at the center of jet flow. With the increase of axial distance (away from the nozzle), the pressure and velocity show a downward trend. In the basic stage, the jet kinetic energy is further consumed. The radial section pressure of jet decreases gradually from the center to the outside. With the increase of axial distance, the velocity and radial pressure continue to show a downward trend, which is like hyperbola. In the dissipation stage, a large amount of air is mixed in the jet and distributed as mist. Currently, the jet pressure and velocity are minimal. The energy exchange between the jet and the environment reaches a balanced state.

2.2 3D model of flow field

As shown in Fig. 1b, the pre-processing software ICEM under ANSYS is used. The three-dimensional model of simulated flow field is established and meshed. After the boundary condition encryption, 942,213 grids are divided. The grid quality is above 0.355. The high-quality grid can meet the requirements of flow field simulation operation.

The nozzle adopts pressure inlet boundary condition. The pressure of outlet is one standard atmosphere. The Eulerian model is selected for the multiphase flow model. The solver selection is based on the pressure solver. The SIMPLE pressure velocity coupling method is adopted. The simulation phase is provided with three phases, namely gas, liquid, and solid. The solid phase is Al_2O_3 or ZrO_2 with average grain size of about 26 μm. Water is the main phase. The weight ratio of spray to water is 1:5. The diameter of the nozzle is 10 mm, and the length of the nozzle is 60 mm. The nozzle contraction angle α is 25°, and the aspect ratio L/D is 6. The initial flow rate is changed with the jet pressure. The turbulence model is standard K-Epsilon. The target surface is 300 mm away from the nozzle exit.

The basic process of simulation is as follows. The high-pressure jet, which is formed by solid particles and water, enters the flow field through the nozzle. Then, the jet impinges on the target surface through the air medium through the flow field. The impact of the abrasive material on the tool surface during micro sandblasting is simulated.

2.3 Micro sandblasting

A wet-type micro sandblasting machine is used in the test. The type of micro sandblasting is 9080-2 W-ZSK (China). The experimental design of wet micro sandblasting process is shown in Fig. 2. The micro sandblasting machine is mainly composed of a sandblasting room, control panel, gun assembly, workpiece fixture, pressure regulating system, and so on. The specific parameters of the abrasive materials (Al_2O_3 and ZrO_2) are shown in Table 1. The blasting angle shall be 90° (vertical injection). The sandblasting method is automatic sandblasting. The installation and clamping mode of the insert is shown in Fig. 2b. The coated insert with AlTiN coating is used for micro sandblasting treatment.
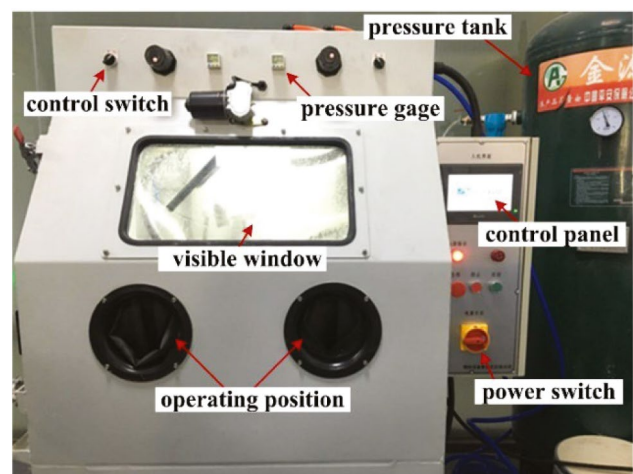
(a)
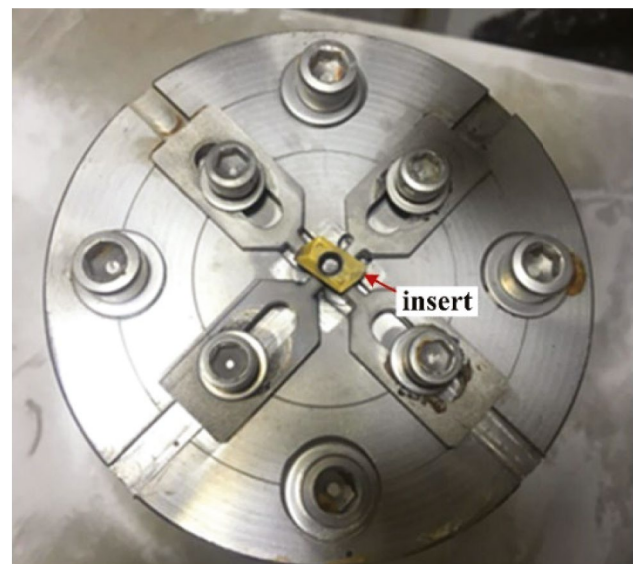
(b)

Fig. 2 Experimental design of wet micro sandblasting process. **a** Equipment and **b** fixture

Table 1 Specific parameters of the abrasive materials

Parameter	Al_2O_3	ZrO_2
Particle size	26 μm	26 μm
Geometrical shape	Polygonal	Globular
Vickers hardness (HV)	2400	1300
Density (g.cm^{-3})	3.6	5.89
Elastic modulus (GPa)	420	300
Yield strength (GPa)	4.8	4
Ultimate strength (GPa)	7	6

Single factor method is adopted to carry out the test. Three test factors are selected with the following parameters: abrasive type of Al_2O_3 and ZrO_2; sandblasting pressure $p = 0, 0.1, 0.3$, and 0.5 MPa; and sandblasting time $t = 0$, 1, 3, 5, and 7 s.

2.4 Cutting experiment

The carbide-coated inserts are produced by Kennametal Company. The coating material is AlTiN, and the brand is KC522M. The tool model of KC522M is EDCT10T304P-DER. The hardness of coating is about 1250 HV. The test results show that the geometric parameters of the insert basically do not change before and after the sandblasting. Therefore, the influence of tool geometric parameters is not considered in the work. The geometric parameters of the insert are shown in Table 2. The indexable end milling cutter produced by Kenner Company was used in the cutting test. The tool rod diameter is 20 mm, and the model is 20A03R028A20ED10. The workpiece material is an iron base superalloy GH2132. Table 3 shows the mechanical properties of GH2132.

2.5 Test methods

After micro sandblasting, a variety of instruments are used to detect the treated tool. Firstly, ultrasonic cleaning instrument is used to clean the treated tool. Then, Quanta250

Table 2 Geometric parameters of the insert KC522M

Model	EDCT10T-304PDER
Rake angle γ_o (°)	8°
Clearance angle α_o (°)	15°
Inclination angle λ_s (°)	15°
Insert length L (mm)	12.05
Insert thickness S (mm)	3.75
Insert width W (mm)	6.75
Corner radius r_ε (mm)	0.40

Table 3 Mechanical properties of GH2132

Heat treatment mode	Tensile strength σ_b (MPa)	Yield strength σ_s (MPa)	Elongation δ (%)	Hardness HRC
Solid solution treatment	930	590	15	36 ± 1

scanning electron microscope (SEM) is used to observe the surface morphology of the treated tool. An optical profiler (model: WYKO NT9300, Germany) is used to measure the surface roughness R_a. In this work, the surface roughness R_a is taken as the average value of five measurements. In addition, X-ray stress analyzer (model: X-3000, Finland) is used to detect the tool surface residual stress. The measured average value of residual stress is selected in the work. The tool failure standard set to the average flank wear VB = 0.3 mm. The flank wear band width was measured by an USB200 tool microscope.

3 Results and discussion

3.1 Flow field erosion simulation analysis

3.1.1 Pressure and velocity of flow field

Figure 3 shows the pressure cloud map and velocity cloud diagram of the flow field at pressure of 0.3 MPa with Al_2O_3 solid phase. As can be seen in Fig. 3a, the water flow enters the flow field from the pressure inlet. When the jet enters the nozzle, the pressure increases sharply, due to the contraction of the inner diameter of the pipe. At the nozzle, outlet pressure reaches the maximum value and tends to be stable. When the jet enters the external flow field (standard atmospheric pressure), the maximum jet pressure is presented in the axial direction. And the pressure distribution spreads out in a "trumpet" shape. As can be seen in Fig. 3b, the velocity reaches its maximum at the jet axis, and the jet velocity presents a scattering state. When the jet enters the external field, the kinetic energy of the jet is gradually affected by air resistance. So, the velocity distribution decreases in the axial and radial direction. When the efflux reaches the target surface through the external flow field, the jet has been blocked by the target surface. So, the minimum of velocity is in the direction of axial and diameter.

Figure 4 shows the variation of pressure and velocity along x axial coordinate, from which can be seen that the same drop law of the jet in the flow field is displayed at different pressures. With the increase of axial distance, the pressure presents a trend of decrease (Fig. 4a). When the jet enters the flow field, it will exchange energy and potential energy with air. The conversion time between potential

Fig. 3 a Pressure and **b** velocity cloud map of the flow field at pressure of 0.3 MPa with Al_2O_3 solid phase


(a)

(b)
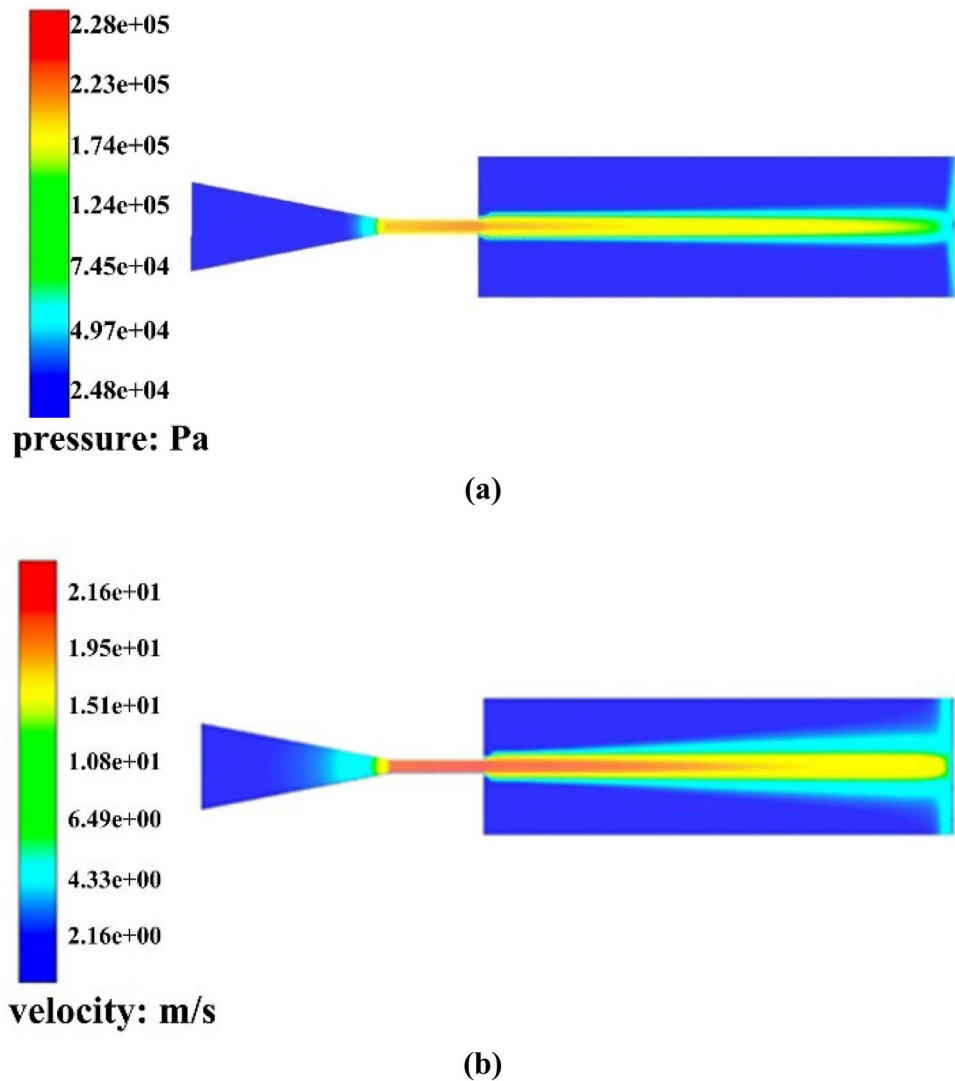
energy is longer with the distance from the nozzle, which leads to the lower pressure at the axis. At any position in the flow field, however, the jet pressure at the axis always keeps at the maximum value of the radial interface (Fig. 3a). As can be seen in Fig. 4b, the velocity at the nozzle is 26 m/s, 23 m/s, and 12.5 m/s when the jet pressure is 0.5 MPa, 0.3 MPa, and 0.1 MPa, respectively. With the increase of x axial distance, the velocity tends to decrease. With the contact between the jet and the target surface, the velocity decreases sharply. As the jet enters the flow field area, the velocity reaches its maximum. With the increase of x axial distance, the kinetic energy gradually exchanges energy with air. And the velocity gradually decreases. The kinetic energy is converted into potential energy, when the mixture of abrasive and water hits the target surface. Thus, the velocity decreases sharply.

To sum up, with the increase of the distance from the nozzle, the jet pressure and velocity all show a downward trend. However, the high pressure of the jet does not indicate the enhancement of the tool surface performance. So, the specific parameter setting needs to be adjusted flexibly according to the actual situation.

3.1.2 Pressure and stress of target surface

Figure 5 shows the pressure cloud map of target surface ($x = 300$ mm). The closer to the center of the target surface is, the greater the pressure is. The pressure away from the center gradually decreases until it disappears. The pressure cloud map presents a symmetric distribution of the center. Although sandblasting pressures are different, the same distribution is presented on the target surface. By contrast, the higher the sandblasting pressure is, the more concentrated the jets are. Because of the scattering of the jet beam, the area of the center circle is larger when the jet impinges on the target surface. Therefore, the pressure on the target
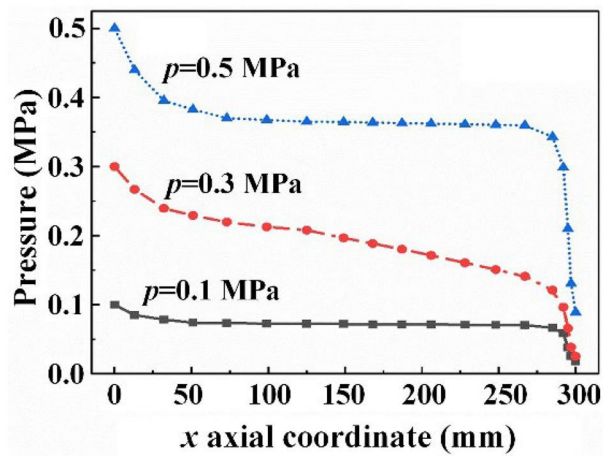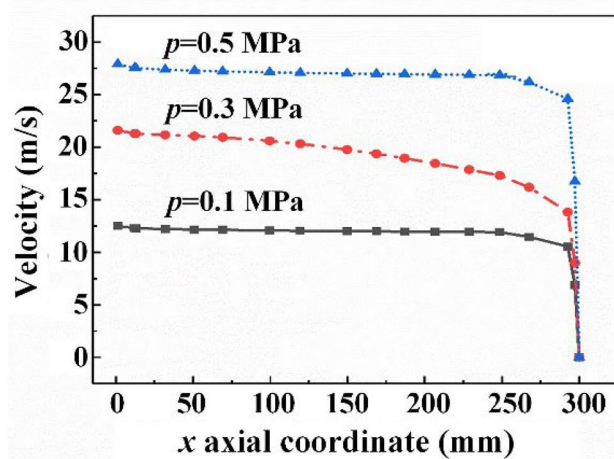
Fig. 4 Variation of **a** pressure and **b** velocity along x axial coordinate ($y=0$, $z=0$, solid phase is Al_2O_3)

Fig. 5 Pressure cloud map of target surface ($x=300$ mm) at **a** $p=0.1$ MPa, **b** $p=0.3$ MPa, and **c** $p=0.5$ MPa

surface decreases with the reduce of sandblasting pressure. The jet beam scatters, and the target pressure decrease from the center to the edge until it disappears.

Figure 6 shows the shear stress cloud map of target surface ($x=300$ mm). The shear stress around the center area is greater than that at the center point. The farther it is from the center of the target plane, the shear stress decreases and disappears. In the actual sandblasting process, the micro-abrasive jet generates shear stress on the target surface. It can not only remove impurity particles on the tool surface, but also improve the surface roughness.

Figure 7 shows the variation of pressure and shear stress along y axial coordinate. The highest pressure is obtained at the center of target surface (Fig. 7a). The pressure at the edge of the target is the lowest and approaches zero. The pressure of jet impinging on the target surface is similar at different sandblasting pressures. The pressure is distributed symmetrically from the center to the edge of the target surface.
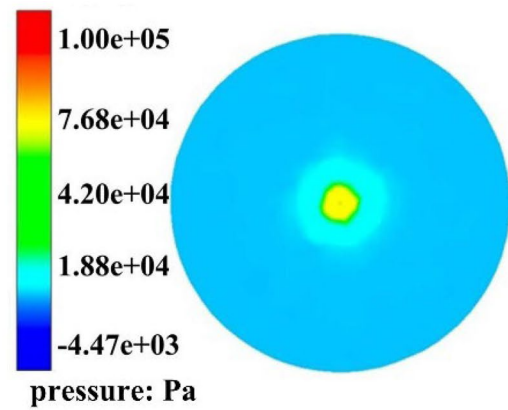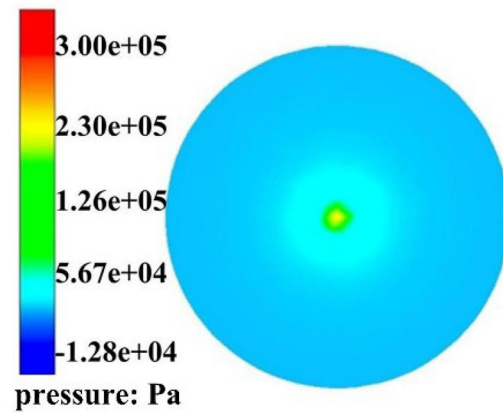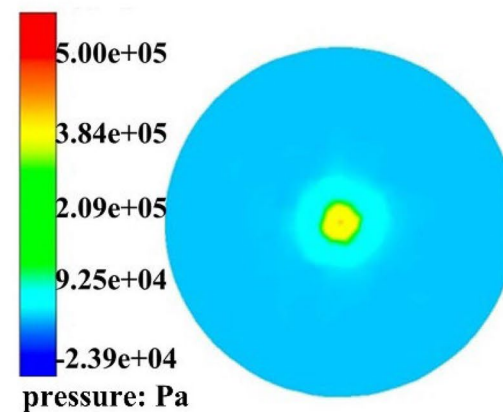
And the pressure curve presents Gaussian normal distribution curve. With the increase of sandblasting pressure, the pressure on the center of the target surface is higher. So, it is suggested that the coated tool should be put in the center of the jet to avoid uneven pressure when jet impinges on tool
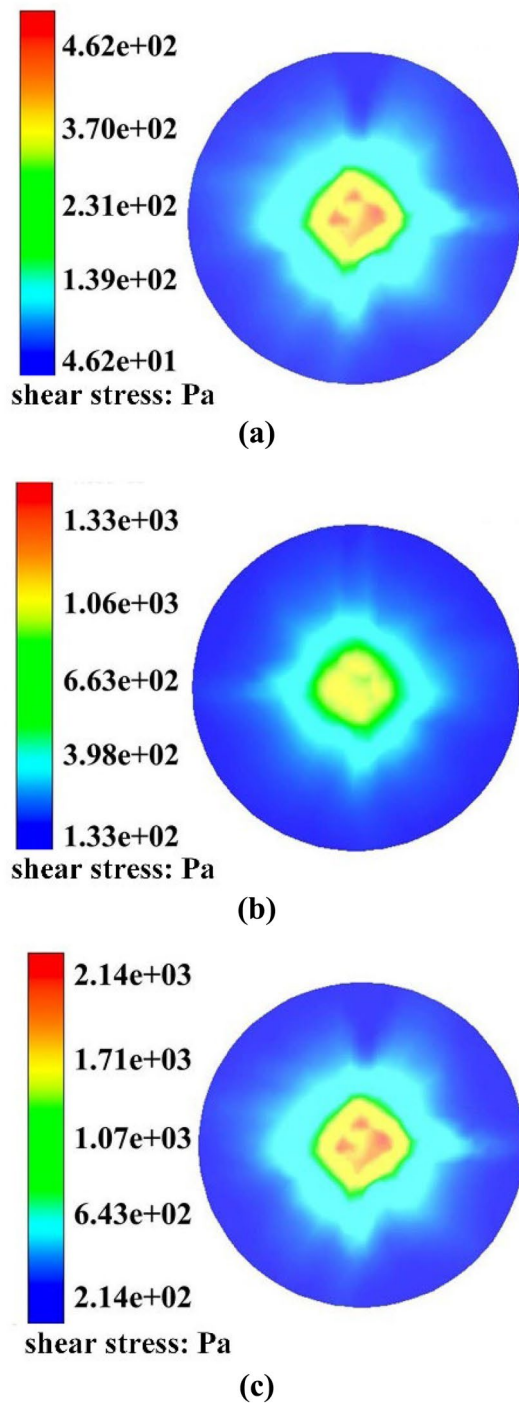
Fig. 6 Shear stress cloud map of target surface ($x = 300$ mm) at **a** $p = 0.1$ MPa, **b** $p = 0.3$ MPa, and **c** $p = 0.5$ MPa

Fig. 7 Variation of **a** pressure and **b** shear stress along y axial coordinate ($x = 300$, $z = 0$, solid phase is Al_2O_3)

surface in the sandblasting process. As can be seen from Fig. 7b, the similar shear stress distribution is presented at different sandblasting pressure, showing a similar "hump" downward trend. The maximum shear stress is not located at the center of the target plane. In a small area around the center of the target plane, the shear stress roughly presents
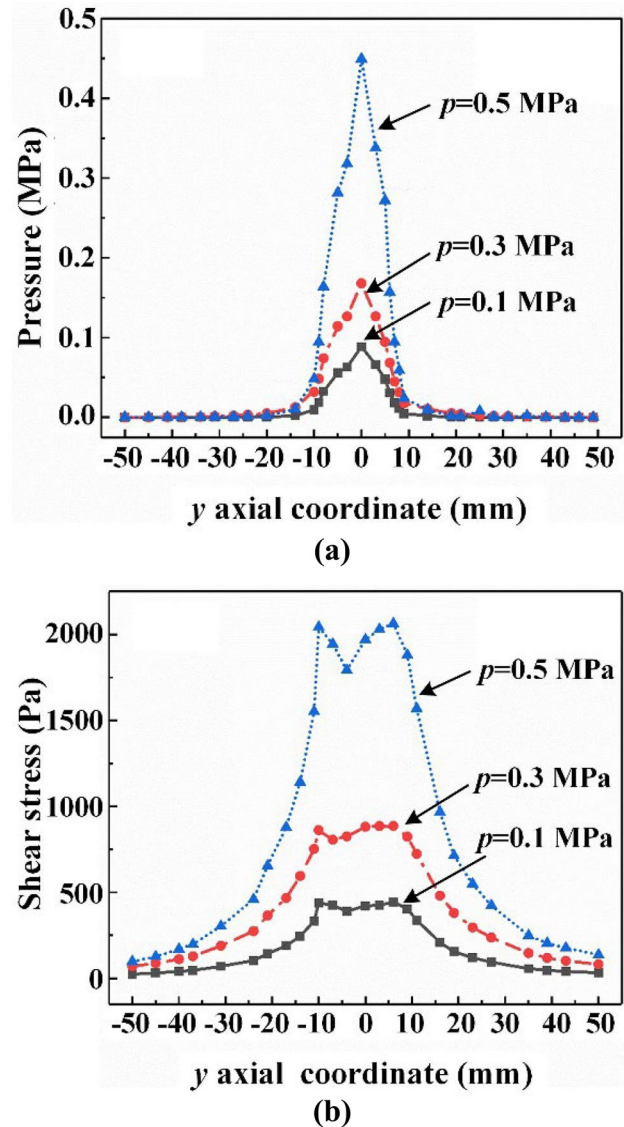
the distribution of the high edge bottom of the center, which is different from the distribution of the stress on the target plane. During the simulation, the target surface is set as an ideal smooth surface with zero initial stress. Therefore, the pressure or shear stress of target surface is low (< 0.5 MPa) in Figs. 4, 5, 6, and 7.

Figure 8 shows the spray distribution cloud map at $x = 100$ mm and $x = 300$ mm. It can be observed that the distribution state of the spray near the nozzle is also symmetrical in the center at $x = 100$ mm (Fig. 8a). Because the jets are relatively concentrated, the injected material is not completely distributed at $x = 100$ mm. The area near the center produces a partial cavity, which results from the fast-injected material in the central area and mixed with some
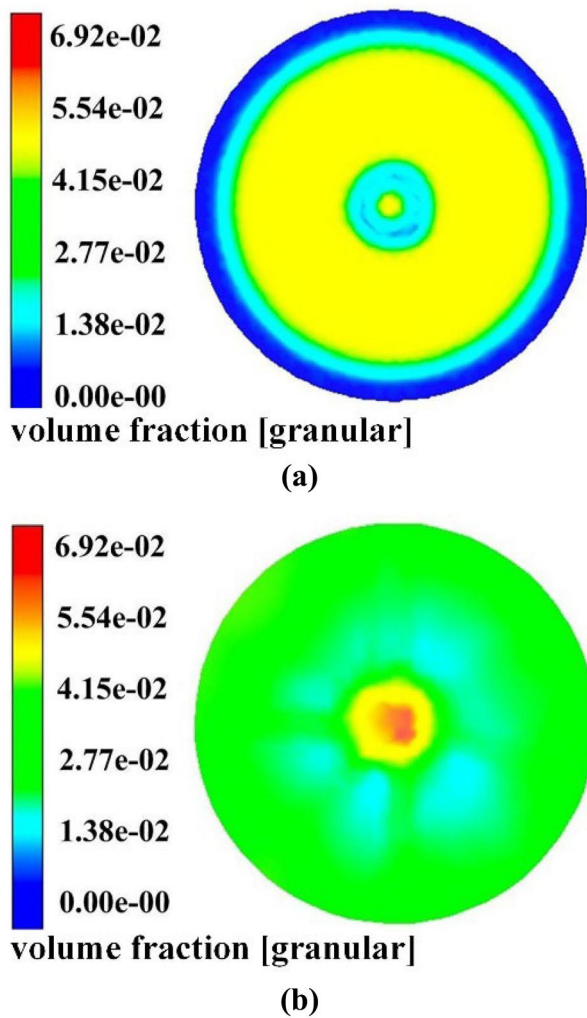
volume fraction [granular]

(a)

volume fraction [granular]

(b)

Fig. 8 Spray distribution cloud map at **a** $x = 100$ mm and **b** $x = 300$ mm

(a)

(b)

Fig. 9 Effect of abrasive on surface morphology of coated tool at $t = 5$ s and $p = 0.3$ MPa. **a** ZrO_2 and **b** Al_2O_3

air. As can be seen from Fig. 8b, the spraying material covers the entire target surface at $x = 300$ mm. When the spray material reaches the target surface, the abrasives exchange energy with air. The kinetic energy of the spraying material is reduced. And the spraying material impacts the target surface in the form of fog. The high area of spray on the target surface is obtained away from the nozzle. The distribution area of the spray decreases with the increase of radial distance. It is suggested that the blasting distance should be controlled reasonably. If it is too close to the nozzle, it causes uneven sandblasting on the tool surface. On the other hand, there is no sandblasting effect at the edge of the tool. If it is too far from the nozzle, the pressure of the injection material on the tool surface will be too small. This is not be able to get the effect of micro sandblasting.

According to the simulation analysis of the pressure and velocity flow field, the flow field erosion model can indirectly simulate the impact of jet on the tool surface.
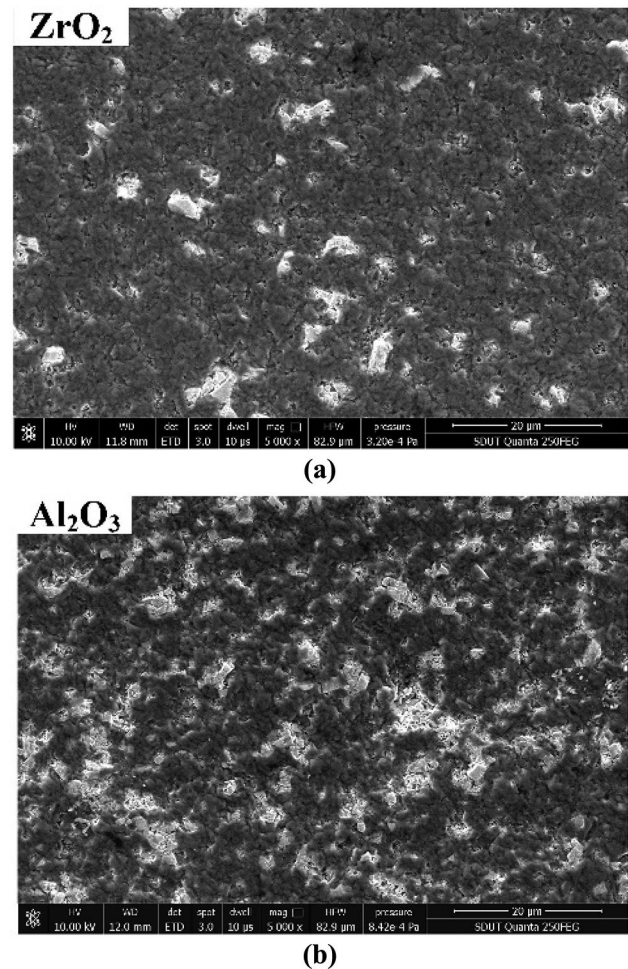
Reasonable prediction and analysis are made on the influence of the tool surface. It can provide a reference for the parameter design of micro sandblasting.

3.2 Surface integrity of the coated tool

3.2.1 Surface morphology

Figure 9 shows the effect of abrasive on surface morphology of coated tool at $t = 5$ s and $p = 0.3$ MPa. The jet is composed of ZrO_2 abrasive and water impinges on the coated tool surface under the push of high-pressure gas (Fig. 9a). The shear stress generated by the jet can remove impurity particles from the coating surface. The white areas are tiny pits left by the impact of the ZrO_2 abrasive (Fig. 9a). As shown in Fig. 9b, the area of white area and the pits on the tool surface are increased, which is caused by the difference in the shape of the Al_2O_3 abrasive. ZrO_2 injection material is spherical structure, while Al_2O_3 is irregular polygonal.

When an irregular prism strikes the surface of the coating, the shape of the abrasive itself will break again, which produce more sharp abrasive. Thus, the sandblasting effect on the coating surface is enhanced. It also leads to an increase in surface roughness. Therefore, Al_2O_3 is more erosive to coatings, which also contributes to a higher removal rate of the coating.

Figure 10 shows the effect of sandblasting pressure and time on surface morphology of coated tool with abrasive of Al_2O_3. At $t = 3$ s, the tiny pits (white areas) appear on the coating surface (Fig. 10b). This is the mark left by the abrasive material hitting the coating surface. At $t = 5$ s, the coating coverage of the tool base layer decreases obviously, and parts of the tool substrate are exposed (Fig. 10c), compared with the untreated coating surface (Fig. 10a). At $t \geq 7$ s, the blasting particles impact the coating for a long time. The

coating disappears completely, and parts of the tool substrate are exposed (Fig. 10d). Therefore, the extension of sandblasting blasting time can cause part of the tool coating to fall off. Then, the tool performance will degrade. At the same time, the thermal protection performance of the coated tool also disappears. During cutting process, the abrasion degree of the tool increases, and the tool life decreases.

Additionally, at $p = 0.1$ MPa, the particle morphology of the coated tool surface significantly disappears and the surface becomes smoother (Fig. 10e), compared with the untreated coating surface (Fig. 10a). When the sandblasting pressure increases to 0.5 MPa (Fig. 10f), the impact of abrasive increases the shedding area of coating. Some parts of the tool substrate leak out. The thermal barrier function of the coating is destroyed, and coating surface defects are correspondingly increased. Just as the simulation results,

Fig. 10 Effect of sandblasting pressure and time on surface morphology of coated tool with abrasive of Al_2O_3
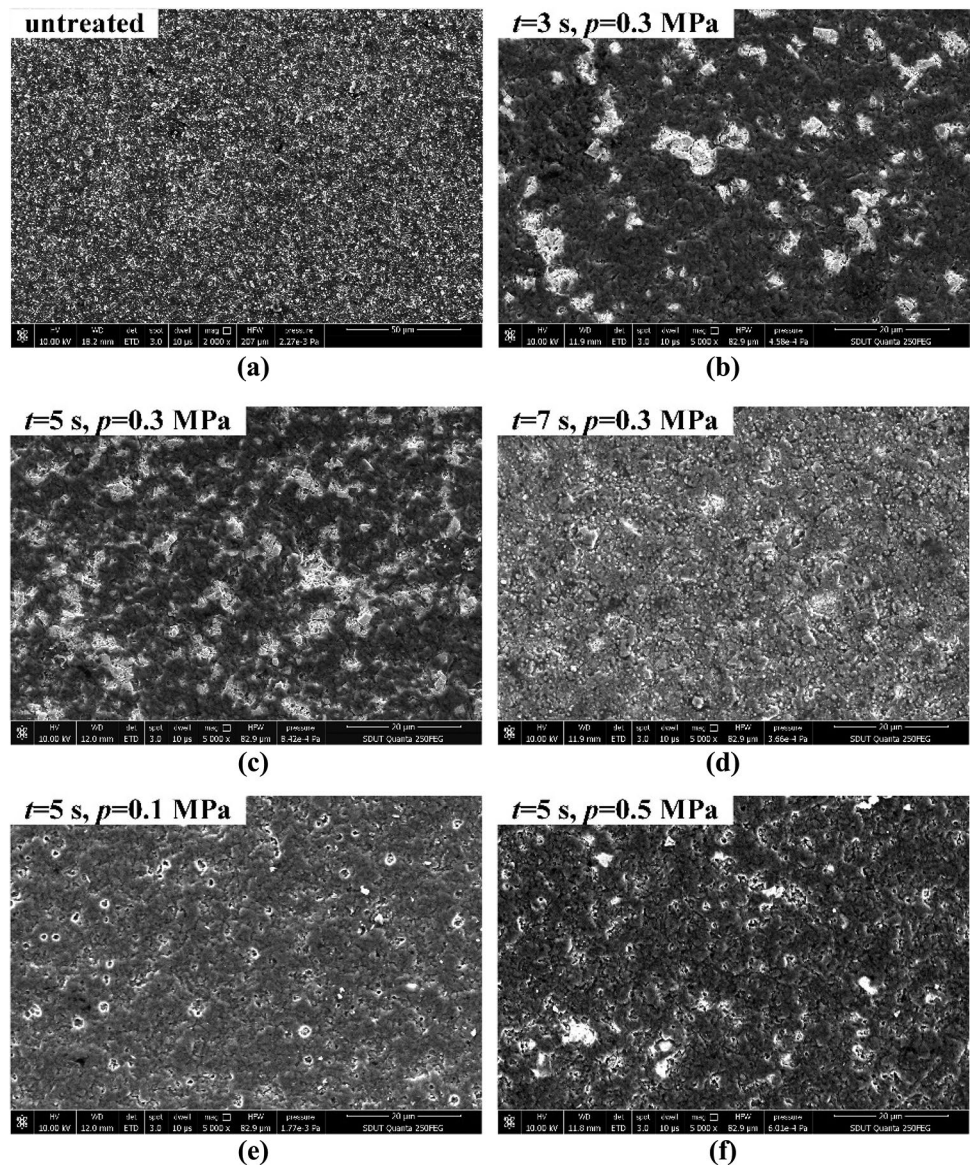
the higher sandblasting pressure can give a strong impact pressure on the tool surface (Figs. 5 and 7). And the shear stress on the tool surface by jet flow is also large (Figs. 6 and 7). If the sandblasting pressure is too low, the impurity particles on the tool surface cannot be removed. It will not have any effect on the tool surface. However, the excessive sandblasting pressure can lead to a strong jet flow, which can produce a large shear stress. It not only affects the cutting performance of the tool, but also reduces its service life.

Therefore, the even surface morphology of the treated coated tool can be obtained at sandblasting pressure $p = 0.1 \sim 0.3$ MPa and sandblasting time $t = 3 \sim 5$ s.

3.2.2 Surface roughness

Figure 11 shows the effect of sandblasting parameters on surface roughness R_a. Under the same micro sandblasting condition, the surface roughness R_a of the coated tool after sandblasting by Al_2O_3 abrasive is 0.423 μm (Fig. 11a), which is higher than that of the untreated tool ($R_a = 0.246$). On the other hand, after ZrO_2 micro sandblasting, the surface roughness R_a is 0.187 μm, which is lower than that of the untreated tool ($R_a = 0.246$). ZrO_2 spray has spherical structure, while Al_2O_3 spray has irregular prismatic structure. The surface roughness R_a of the tool treated by Al_2O_3 is higher than that treated by ZrO_2. Al_2O_3 spray has sharp edges and corners. When irregular edges hit the coating surface, the spray will break again and create more edges. This results in increased roughness of the tool surface. It is verified that Al_2O_3 abrasive has a stronger impact on the coating.

As can be seen from Fig. 11b, with the increase of sandblasting pressure, the surface roughness R_a presents a rising trend. As the sandblast pressure increases, the impact force of the abrasive against the tool surface is improved. When the abrasive hits the tool surface, the solid impurities will be removed from the tool surface. However, the sharp edges and corners of Al_2O_3 itself can damage the coating surface. Part of the coating is detached from the tool substrate. This results in a larger value of the surface roughness R_a. The surface roughness R_a is 0.528 μm at $p = 0.5$ MPa. The reason for the increase of surface roughness R_a is the coating falling off. Therefore, a suitable pressure range can avoid the erosion of coating.

As shown in Fig. 11c, the minimum surface roughness R_a is obtained at $t = 1$ s with the abrasive material of Al_2O_3, while it is obtained at $t = 7$ s with the abrasive material of ZrO_2. The sharp part of Al_2O_3 abrasive causes the impurity particles on the coating surface to be removed first at $t = 1$ s. So the surface roughness is reduced. At $t = 3$ s, the Al_2O_3 abrasive hitting the coating surface will produce large pits, increasing surface roughness. When the sandblasting time exceeds 3 s, the coating removal rate and the number of shallow surface pits are enhanced. Therefore, the surface roughness
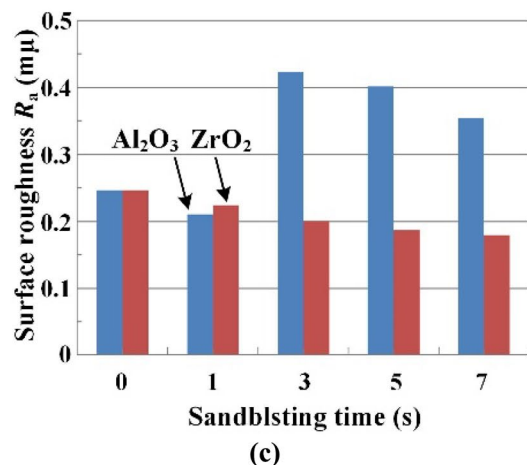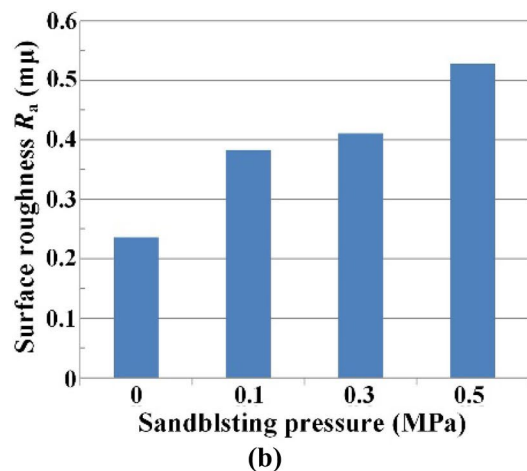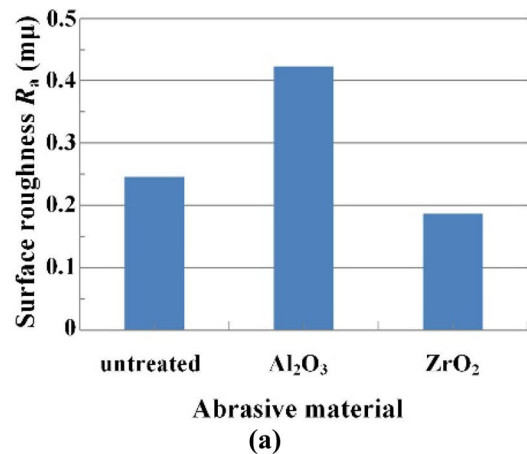

Fig. 11 Effect of sandblasting parameters on surface roughness R_a, **a** $t = 5$ s and $p = 0.3$ MPa, **b** Al_2O_3 and $t = 5$ s, and **c** $p = 0.3$ MPa

R_a is decreased, and the coating surface becomes smoother. On the other hand, with the extension of sandblasting time, the surface roughness R_a shows a decreasing trend when ZrO_2 abrasive is used. Only small pits are induced by ZrO_2 abrasive. The deposition particles and defects on the coating

surface are eliminated. The surface becomes smoother, and the surface roughness R_a is decreased.

Therefore, the high surface roughness R_a can be contributed by Al_2O_3 abrasive at high sandblasting pressure and long sandblasting time.

3.2.3 Surface residual stress

Figure 12 shows the effect of sandblasting parameters on residual stress. The initial residual stress on the tool surface without micro sandblasting is −667 MPa, which is induced by manufacturing process. In the process of micro sandblasting, the jet composed of abrasive and water continuously impinges on the tool surface. The previous simulation results show that the high-pressure jet will have a strong impact force on the tool surface. The residual stress level on the coated tool surface is enhanced accordingly. On the other hand, the sandblasting process cannot only remove the impurities on the tool surface, but also enhance the surface compactness. When the injection time is prolonged or the sandblasting pressure is increased, the residual stress on the tool surface is increased again. So, the residual stress of the tool itself combined with the residual stress after sandblasting will result in the final residual stress greater than 300 MPa.

As can be seen in Fig. 12a, the residual stress on the tool surface treated by Al_2O_3 is − 864 MPa, increasing by about 29.5% compared with that of the untreated tool ($\sigma_r = -667$ MPa). After ZrO_2 treatment, the tool surface residual stress σ_r is −748 MPa, which is increased by 12.1%. The residual stress on the tool surface treated by Al_2O_3 is higher than that treated by ZrO_2. This is mainly contributed by the sharp edges and corners of the Al_2O_3 spray. The sharp multi-angle edge particles impact the tool surface, which has a strengthening effect on the coating. Therefore, Al_2O_3 has stronger erosion ability on coating than ZrO_2. During high-speed cutting process, the higher residual compressive stress can inhibit the formation of microcracks on the tool surface. Thus, the cutting performance of the tool can be improved.

As can be seen in Fig. 12b, with the increase of sandblasting pressure, the compressive stress (absolute value) presents a trend of first increasing and then decreasing. The impact of jet beam is not only conducive to the removal of impurity particles on the tool surface, but also can increase the residual stress on the tool surface. The greater the jet pressure is, the greater the impact strength on the tool surface will be. So, the highest residual stress (absolute value) is obtained at $p = 0.3$ MPa. Once the sandblasting pressure exceeds 0.3 MPa, the strong jet pressure accompanied by the spray particles can remove part of the tool coating material. The reduction of coating thickness can cause part of the coating to fall off from substrate. Thus, the surface
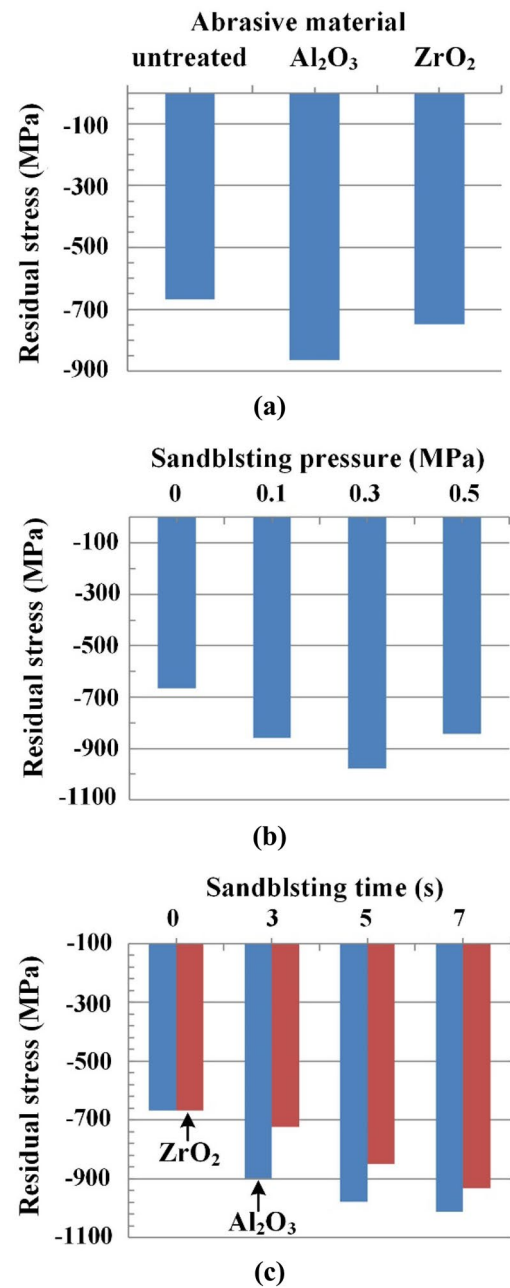

Fig. 12 Effect of sandblasting parameters on residual stress, **a** $t = 5$ s and $p = 0.3$ MPa, **b** Al_2O_3 and $t = 5$ s, and **c** $p = 0.3$ MPa

residual compressive stress (absolute value) is reduced at $p = 0.5$ MPa.

As can be seen in Fig. 12c, with the extension of sandblasting time, the residual compressive stress (absolute value) on the tool surface is enhanced. The abrasive particles are constantly bumping into the coating surface. The impact on the tool surface is stronger due to the Al_2O_3 abrasive with sharp shape. The surface residual compressive stress (absolute value) is significantly increased.

According to the above results, the high level of surface integrity (e.g., low surface roughness R_a, even surface morphology and high residual compressive stress (absolute value)) for the AlTiN-coated tool can result from sandblasting pressure $p = 0.1 \sim 0.3$ MPa and sandblasting time $t = 3–5$ s with Al_2O_3 abrasive.

3.3 Cutting performance of coated tools

The effect of sandblasting parameters on tool life is exhibited in Fig. 13. Compared with the untreated tool life (10.9 min), the tool life (16.5 min) of coated tool after treating of $p = 0.2$ MPa and $t = 2$ s is improved by about 50% at $v_c = 180$ m/min, while the tool life (21.8 min) of coated tool after treating of $p = 0.3$ MPa and $t = 3$ s is improved by about 100%. On the other hand, at $v_c = 120$ m/min, the tool life (18.3 min) of coated tool after treating of $p = 0.2$ MPa and $t = 2$ s is improved by about 22%, while the tool life (20.1 min) of coated tool after treating of $p = 0.3$ MPa and $t = 3$ s is improved by about 33% (Fig. 13a), compared with the untreated tool life (15 min).

With the increase of sandblasting pressure, the tool life first increases and then decreases (Fig. 13b). At $p = 0.1 \sim 0.3$ MPa, the impurity particles are removed from the coating surface. The high residual stress (absolute value) induced by the sandblasting pressure at $p = 0.1 \sim 0.3$ MPa (Fig. 12) leads to the improvement of tool surface performance. At $p \geq 0.3$ MPa, the excessive sandblasting pressure can destroy the tool coating, which can result in weakening the surface integrity and reducing the tool life. So, the suitable micro sandblasting treatment can prolong the service life of the tool. As shown in Fig. 13c, the tool life tends to decrease with the increase of sandblasting time. The residual compressive stress introduced by micro sandblasting helps to reduce the generation of microcracks in the cutting process. The longtime jet impact can reduce the thickness of the tool coating. It may even expose the substrate of the coating tool. So, longtime spray impact is not conducive to tool surface strengthening and affect tool life.

At the same cutting parameters, the tool life of the blasted tool is higher than that without sandblasting. When the sandblasting parameters are different, the tool life improvement

Fig. 13 Effect of sandblasting parameters on tool life, **a** KC522M, **b** and **c** $v_c = 180$ m/min, $f_z = 0.04$ mm/z, $a_p = 0.4$ mm, $a_e = 3$ mm
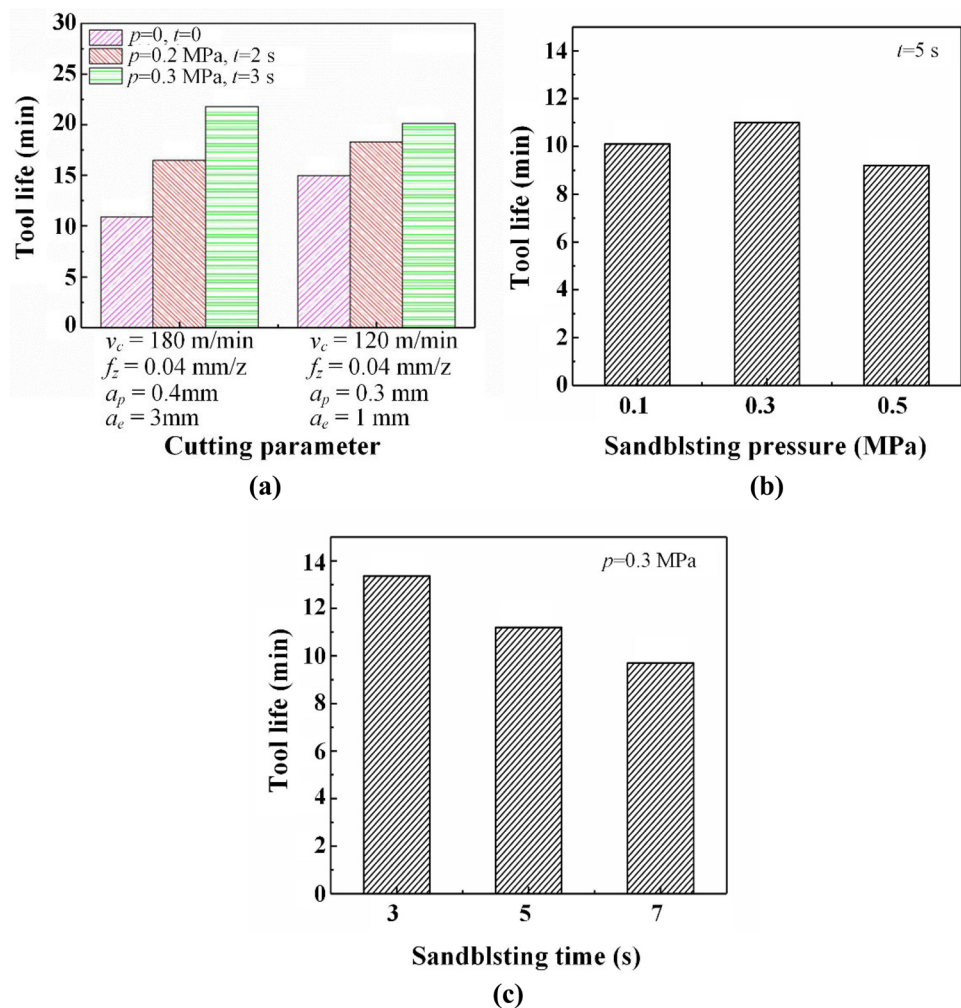
level is different. The higher tool life can be achieved for the AlTiN coated tool at $p = 0.3$ MPa and $t = 3$ s.

The coating thickness, hardness, and adhesive strength are also important indicators of surface integrity. The research shows that the film thickness may decrease due to the abrasion phenomena activated after micro-blasting process [9]. The flank wear VB decreases with the improvement of dimensionless thickness. However, it becomes a small constant when the ratio increases to a certain level [24]. Additionally, the adhesive strength of coating is obviously enhanced by the sandblasting pretreatment [25]. In this work, the research on the surface integrity of the coating focuses on the surface roughness and residual stress. The influence of coating thickness and adhesive strength is mainly shown by the cutting test results. In addition, the hardness of coating is about 1250 HV, which is changed little before and after sandblasting. In the future work, we will focus on the research of coating thickness, adhesive strength, and hardness.

4 Conclusion

1. When the jet enters the external flow field (standard atmospheric pressure), the maximum of the velocity and pressure is obtained at the center of jet flow. The pressure and the shear stress on the target surface are decreased from the center to edge until it disappears. The shear stress around the center area of the target surface is larger than the shear stress at the center point.
2. With the extension of micro sandblasting time, the deposition particles and defects on the coating surface are eliminated. And the surface roughness R_a is reduced. Under the same sandblasting parameters, the residual compressive stress on the tool surface is increased to a higher level when Al_2O_3 abrasive is used.
3. For the AlTiN coated tool, the high level of surface integrity can be caused by Al_2O_3 abrasive at $p = 0.1 \sim 0.3$ MPa and $t = 3\text{–}5$ s.
4. At the same cutting parameters, the tool life of the blasted tool is higher than that without sandblasting. The higher tool life can be achieved for the AlTiN-coated tool at $p = 0.3$ MPa and $t = 3$ s.

Author contribution Zhou Yu: conceptualization, methodology, formal analysis, investigation, writing (original draft), and writing (review and editing). Yujuan Dong: methodology and writing (review and editing). Guangming Zheng: investigation, formal analysis, writing (review and editing), and supervision. Xiuli Jiang: writing—review and editing. Xiang Cheng: methodology and formal analysis. Xianhai Yang: methodology, investigation, and formal analysis. Kaishuo Chang: writing—review and editing. Xuewei Li: methodology and formal analysis.

Declarations

Ethics approval Not applicable.

Consent to participate Not applicable.

Consent for publication The copyright permission has been taken, and consent to submit has been received explicitly from all authors.

Competing interests The authors declare no competing interests.

References

1. Azim S, Gangopadhyay S, Mahapatra SS, Mittal R, Singh RK (2020) Role of PVD coating on wear and surface integrity during environment-friendly micro-drilling of Ni-based superalloy. J Clean Prod 272:122741. https://doi.org/10.1016/j.jclepro.2020.122741
2. Zoei MS, Sadeghi MH, Salehi M (2016) Effect of grinding parameters on the wear resistance and residual stress of HVOF-deposited WC-10Co-4Cr coating. Surf Coat Technol 307:886–891. https://doi.org/10.1016/j.surfcoat.2016.09.067
3. Bouzakis K-D, Charalampous P, Kotsanis T, Skordaris G, Bouzakis E, Denkena B, Breidenstein B, Aurich JC, Zimmermann M, Herrmann T, M'saoubi R (2017) Effect of HM substrates' cutting edge roundness manufactured by laser machining and micro-blasting on the coated tools' cutting performance. CIRP J Manuf Sci Technol 18:188–197. https://doi.org/10.1016/j.cirpj.2017.02.003
4. Yunata EE, Aizawa T, Tamaoki K, Kasugi M (2017) Plasma polishing and finishing of cvd-diamond coated WC (Co) dies for dry stamping. Procedia Eng 207:2197–2202. https://doi.org/10.1016/j.proeng.2017.10.981
5. Qin Y, Zhao H, Li C, Lu J, He J (2020) Effect of heat treatment on the microstructure and corrosion behaviors of reactive plasma sprayed TiCN coatings. Surf Coat Technol 398:126086. https://doi.org/10.1016/j.surfcoat.2020.126086
6. Giti R, Haghdoost S, Ansarifard E (2020) Effect of different coloring techniques and surface treatment methods on the surface roughness of monolithic zirconia. Dent Res J 17:152–161. https://doi.org/10.4103/1735-3327.280893
7. Jacoba A, Gangopadhyay S, Satapathy A, Mantry S, Jhab BB (2017) Influences of micro sandblasting as surface treatment technique on properties and performance of the AlTiN coated tools. J Manuf Process 29:407–418. https://doi.org/10.1016/j.jmapro.2017.08.013
8. Bouzakis K-D, Klocke F, Skordaris G, Bouzakis E, Gerardis S, Katirtzoglou G, Makrimallakis S (2011) Influence of dry micro-blasting grain quality on wear behaviour of TiAlN coated tools. Wear 271:783–791. https://doi.org/10.1016/j.wear.2011.03.010
9. Bouzakis K-D, Skordaris G, Bouzakis E, Tsouknidas A, Makrimallakis S, Gerardis S, Katirtzoglou G (2011) Optimization of wet micro-blasting on PVD films with various grain materials for improving the coated tools' cutting performance. CIRP Ann Manuf Technol 60:587–590. https://doi.org/10.1016/j.cirp.2011.03.012
10. Abusuilik SB, Inoue K (2013) Effects of intermediate surface treatments on corrosion resistance of cathodic arc PVD hard coatings. Surf Coat Technol 237:421–428. https://doi.org/10.1016/j.surfcoat.2013.09.026

11. Abusuilik SB (2015) Pre-, intermediate, and post-treatment of hard coatings to improve their performance for forming and cutting tools. Surf Coat Technol 284:384–395. https://doi.org/10.1016/j.surfcoat.2015.07.003

12. Chang K, Zheng G, Cheng X, Xu R, Li Y, Yu Z, Yang X (2021) Surface integrity evolution and wear evolution of the micro-blasted coated tool in high-speed turning of Ti6Al4V. Int J Adv Manuf Technol 115:603–616. https://doi.org/10.1007/s00170-021-07227-8

13. Petrogalli C, Montesano L, Pola A, Gelfi M, Ghidini A, LaVecchiaa GM (2015) Improvement of fatigue resistance of a tool steel by surface treatments. Procedia Eng 109:154–161. https://doi.org/10.1016/j.proeng.2015.06.227

14. Tanaka S, Shirochi T, Nishizawa H, Metoki K, Miura H, Hara H, Takahashi T (2016) Micro-blasting effect on fracture resistance of PVD-AlTiN coated cemented carbide cutting tools. Surf Coat Technol 308:337–340. https://doi.org/10.1016/j.surfcoat.2016.07.094

15. Puneet C, Valleti K, Gopal AV (2017) Influence of surface preparation on the tool life of cathodic arc PVD coated twist drills. J Manuf Process 27:233–240. https://doi.org/10.1016/j.jmapro.2017.05.011

16. Liu C, Liu Z, Wang B (2018) Modification of surface morphology to enhance tribological properties for CVD coated cutting tools through wet micro blasting post-process. Ceram Int 44:3430–3439. https://doi.org/10.1016/j.ceramint.2017.11.142

17. Shen T, Zhu L, Liu Z (2020) Effect of micro-blasting on the tribological properties of TiN/MT-TiCN/Al$_2$O$_3$/TiCNO coatings deposited by CVD. Int J Refract Metal Hard Mater 88:105205. https://doi.org/10.1016/j.ijrmhm.2020.105205

18. Mundotia R, Kothari DC, Kale A, Mhatre U, Date K, Thorat N, Ghorudea T (2020) Effect of ion bombardment and micro sand-blasting on the wear resistance properties of hard TiN coatings. Mater Today Proc 26:603–612. https://doi.org/10.1016/j.matpr.2019.12.171

19. Faksa L, Daves W, Ecker W, Klünsner T, Tkadletz M, Czettl C (2019) Effect of shot peening on residual stresses and crack closure in CVD coated hard metal cutting inserts. Int J Refract Metal Hard Mater 82:174–182. https://doi.org/10.1016/j.ijrmhm.2019.04.008

20. Gruber DP, Kiefer D, Rössler R, Beckmann F, Tkadletz M, Klünsner T, Czettl C, Keckes J, Gibmeier J (2019) 20 Hz synchrotron X-ray diffraction analysis in laser-pulsed WC-Co hard metal reveals oscillatory stresses and reversible composite plastificationm. Int J Refract Metal Hard Mater 82:121–128. https://doi.org/10.1016/j.ijrmhm.2019.04.004

21. Thakur RK, Singh KK (2020) Experimental investigation and optimization of abrasive water jet machining parameter on multi-walled carbon nanotube doped epoxy/carbon laminate. Measurement 164:108093. https://doi.org/10.1016/j.measurement.2020.108093

22. Bouzakis K-D, Makrimallakis S, Katirtzoglou G, Skordaris G, Gerardis S, Bouzakis E, Leyendecker T, Bolz S, Koelkerc W (2010) Adaption of graded Cr/CrN-interlayer thickness to cemented carbide substrates' roughness for improving the adhesion of HPPMS PVD films and the cutting performance. Surf Coat Technol 205:1564–1570. https://doi.org/10.1016/j.surfcoat.2010.09.010

23. Melentiev R, Fang F (2019) Investigation of erosion temperature in micro-blasting. Wear 420–421:123–132. https://doi.org/10.1016/j.wear.2018.12.073

24. Bar-Hen M, Etsion I (2017) Experimental study of the effect of coating thickness and substrate roughness on tool wear during turning. Tribol Int 110:341–347. https://doi.org/10.1016/j.triboint.2016.11.011

25. Shen X, Wang X, Sun F, Ding C (2017) Sandblasting pretreatment for deposition of diamond films on WC-Co hard metal substrates. Diam Relat Mater 73:7–14. https://doi.org/10.1016/j.diamond.2016.10.025